Travelling wave solutions in a negative nonlinear diffusion-reaction model

Yifei Li[1] · **Peter van Heijster**[1] · **Robert Marangell**[2] · **Matthew J. Simpson**[1]

Abstract We use a geometric approach to prove the existence of smooth travelling wave solutions of a nonlinear diffusion-reaction equation with logistic kinetics and a convex nonlinear diffusivity function which changes sign twice in our domain of interest. We determine the minimum wave speed, c^*, and investigate its relation to the spectral stability of the travelling wave solutions.

1 Introduction

Invasion processes have been studied with mathematical models, especially partial differential equations (PDEs), for many years; see, for example, [32] and references therein. These models describe, for instance, how cells are transported to new areas in which they persist, proliferate, and spread [28]. To incorporate information about individual-level behaviours in invasion processes, lattice-based discrete models are widely used [10, 20, 19, 43]. In these discrete models, individual agents are permitted to move, proliferate and die on a lattice, and the average density of agents is related to PDE descriptions obtained using truncated Taylor series in the continuum limit [2, 6]. The macroscopic behaviour described by the PDEs in terms of expected agent density reflects the individual microscopic behaviour. Travelling wave solutions are of particular interest among the macroscopic behaviours arising from these continuum models, as they reflect various modes of microscopic invasive behaviours. One famous model exhibiting travelling wave solutions is the Fisher-KPP equation (KPP refers to Kolmogorov, Petrovsky, Piskunov) proposed in 1937 to study population dynamics with linear diffusion and logistic growth [15, 25]. The existence and stability of travelling wave solutions of the Fisher-KPP equation has been widely studied, see, for instance, [4, 15, 18, 25, 27, 32].

The Fisher-KPP equation can be derived as a continuum limit of a discrete model under the assumption that the population of cells can be treated as a uniform population without any differences in subpopulations [5]. However, differences between individual and collective behaviour have been observed in cell biology and ecology in practice. For instance, in cell biology, isolated cells called *leader cells* are more motile than the grouped cells, called *follower cells* [34]. Also, contact interactions lead to different motility rates between isolated cells and grouped cells in the migration of breast cancer cells [43, 44], glioma cells [24], would healing processes [23] and the development of the enteric nervous system [12]. In ecology, the population growth rate of some species decreases

[1] School of Mathematical Sciences, Queensland University of Technology, Brisbane, Australia

[2] School of Mathematics and Statistics, University of Sydney, Sydney, Australia

as their populations reach small sizes or low densities [7]. This phenomenon is usually referred to as the Allee effect [1].

To describe the invasion process and reflect the difference between collective and individual behaviour, Johnston and coworkers introduced a discrete model considering birth, death and movement events of agents that are isolated or grouped on a simple one-dimensional lattice [20]. A discrete conservation statement describing δU_j, which is the change of the occupancy of a lattice site j during a time step τ, gives

$$\begin{aligned}\delta U_j =& \frac{P_m^i}{2}[U_{j-1}(1-U_j)(1-U_{j-2}) + U_{j+1}(1-U_j)(1-U_{j+2}) \\ &- 2U_j(1-U_{j-1})(1-U_{j+1})] \\ &+ \frac{P_m^g}{2}[U_{j-1}(1-U_j) + U_{j+1}(1-U_j) - U_j(1-U_{j-1}) - U_j(1-U_{j+1})] \\ &- \frac{P_m^g}{2}[U_{j-1}(1-U_j)(1-U_{j-2}) + U_{j+1}(1-U_j)(1-U_{j+2}) \\ &- 2U_j(1-U_{j-1})(1-U_{j+1})] \\ &+ \frac{P_p^i}{2}[U_{j-1}(1-U_j)(1-U_{j-2}) + U_{j+1}(1-U_j)(1-U_{j+2})] \\ &+ \frac{P_p^g}{2}[U_{j-1}(1-U_j) + U_{j+1}(1-U_j)] \\ &- \frac{P_p^g}{2}[U_{j-1}(1-U_j)(1-U_{j-2}) + U_{j+1}(1-U_j)(1-U_{j+2})] \\ &- P_d^i[U_j(1-U_{j-1})(1-U_{j+1})] - P_d^g U_j + P_d^g[U_j(1-U_{j-1})(1-U_{j+1})].\end{aligned} \tag{1}$$

Here, U_j represents the probability that an agent occupies lattice j, thus, $1-U_j$ represents the probability that lattice j is vacant [41]. P_m^i and P_m^g represents the probability per time step that isolated or grouped agent, respectively, attempts to step to a nearest neighbour lattice site; P_p^i and P_p^g represents the probability per time step that an isolated or grouped agent, respectively, attempts to undergo a proliferation event and deposit a daughter agent at a nearest neighbour lattice site; P_d^i and P_d^g represents the probability per time step that an isolated or grouped agent, respectively, dies, and is removed from the lattice. See Figure 1a for a schematic of the lattice-based discrete model.

To obtain a continuous description, Johnston and coworkers treated U_j as a continuous function, $U(x,t)$, and divide (1) by the time step τ. Next, they expanded all terms in (1) in a Taylor series around $x = j\Delta$, where Δ is the lattice spacing, and neglect terms of $\mathcal{O}(\Delta^3)$ [41]. As $\Delta \to 0$ and $\tau \to 0$ with the restriction that the ratio Δ^2/τ held constant [6, 41], they obtained a nonlinear diffusion-reaction equation

$$\frac{\partial U}{\partial t} = \frac{\partial}{\partial x}\left(D(U)\frac{\partial U}{\partial x}\right) + R\left(U\right), \tag{2}$$

where

$$D\left(U\right) = D_i\left(1 - 4U + 3U^2\right) + D_g\left(4U - 3U^2\right), \tag{3}$$

is the nonlinear diffusivity function, and

$$R\left(U\right) = \lambda_g U\left(1-U\right) + \left(\lambda_i - \lambda_g - K_i + K_g\right)U\left(1-U\right)^2 - K_g U, \tag{4}$$

is the kinetic term. Furthermore, the parameters are given by

$$D_g = \lim_{\Delta,\tau\to 0}\frac{P_m^g\Delta^2}{2\tau}, \qquad D_i = \lim_{\Delta,\tau\to 0}\frac{P_m^i\Delta^2}{2\tau}, \qquad \lambda_g = \lim_{\tau\to 0}\frac{P_p^g}{\tau},$$
$$\lambda_i = \lim_{\tau\to 0}\frac{P_p^i}{\tau}, \qquad K_g = \lim_{\tau\to 0}\frac{P_d^g}{\tau}, \qquad K_i = \lim_{\tau\to 0}\frac{P_d^i}{\tau},$$

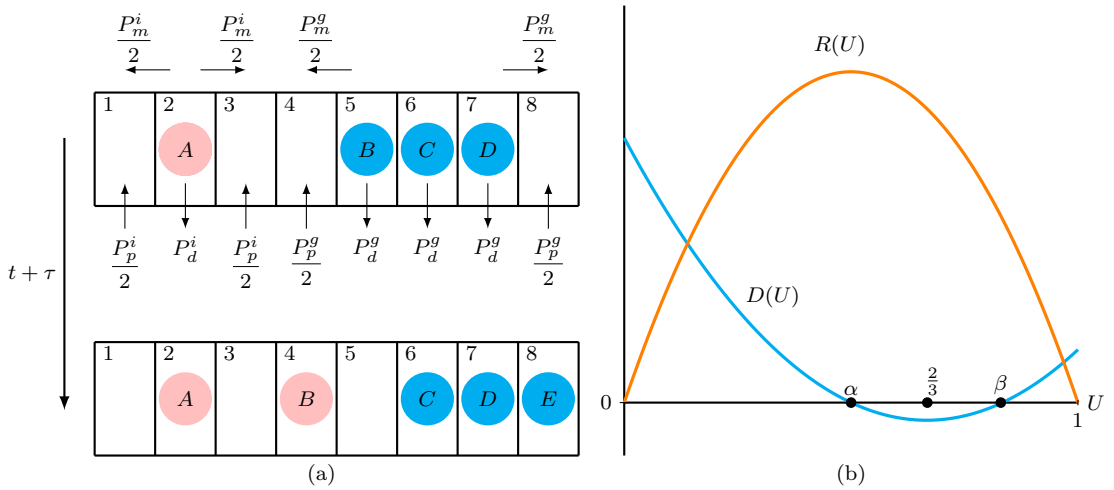

Fig. 1 (a) describes one possible time step of the lattice-based discrete model of [20]: a new grouped agent (agent E) is born and the grouped agent B moves from lattice site 5 to lattice site 4 to become an isolated agent. Pink circles represent isolated agents with birth rate P_p^i, death rate P_d^i and motility rate related to P_m^i; cyan circles represent grouped agents with birth rate P_p^g, death rate P_d^g and motility rate P_m^g. (b) presents a diffusivity function $D(U)$, given by (3) (cyan curve) satisfying $D_i > 4D_g$ which makes $D(U)$ change sign twice on $(0,1)$, and the kinetic term $R(U)$, given by (5) (orange curve) which is positive on $(0,1)$ and zero at end points $U = 0$ and $U = 1$.

where we require that $P_p^i, P_p^g, P_d^i, P_d^g$ are $\mathcal{O}(\tau)$ [41]. Here, $U(x,t)$ denotes the total density of the agents at position $x \in \mathbb{R}$ and time $t \in \mathbb{R}_+$; $D_i \geq 0$ and $D_g \geq 0$ are diffusivities of the isolated and grouped agents, respectively; $\lambda_i \geq 0$ and $\lambda_g \geq 0$ are the birth rates of isolated and grouped agents, respectively; $K_i \geq 0$ and $K_g \geq 0$ are the death rates of isolated and grouped agents, respectively [20].

In this manuscript, we study the effect that aggregation, which is modelled with a nonlinear diffusivity function that goes negative [42], has on the dynamics of the model. Therefore, we assume that $D_i > 4D_g$ such that $D(U)$ given by (3) is convex and changes sign twice in our domain of interest (however, see Section 4.2 for a short discussion related to the other case). For simplicity, we furthermore assume equal proliferation rates, $\lambda = \lambda_i = \lambda_g$, and no agent death, $K_i = K_g = 0$. This way, the kinetic term simplifies to a logistic term

$$R(U) = \lambda U(1-U), \tag{5}$$

and $D(U)$ has a sign condition:

$$D(U) > 0 \quad \text{for} \quad U \in [0,\alpha) \cup (\beta,1], \quad D(U) < 0 \quad \text{for} \quad U \in (\alpha,\beta), \tag{6}$$

where the interval where $D(U) < 0$ is centred around $U = 2/3$, and α, β are given by

$$\alpha = \frac{2}{3} - \frac{\sqrt{D_i^2 + 4D_g^2 - 5D_iD_g}}{3(D_i - D_g)}, \quad \beta = \frac{2}{3} + \frac{\sqrt{D_i^2 + 4D_g^2 - 5D_iD_g}}{3(D_i - D_g)}, \tag{7}$$

with $1/3 < \alpha < 2/3$ and $2/3 < \beta < 1$, see Figure 1b. That is, we have negative diffusion for $U \in (\alpha,\beta)$. The relation that D_i is larger than D_g indicates that isolated agents are more active than grouped agents, which agrees with the experimental observation that *leader cells* are more motile than *follower cells* [34, 44].

[13] showed the existence of travelling wave solutions for a range of positive wave speeds for (2) with general convex $D(U)$ that changes sign twice on $(0,1)$ and $R(U)$ given by (5) based on

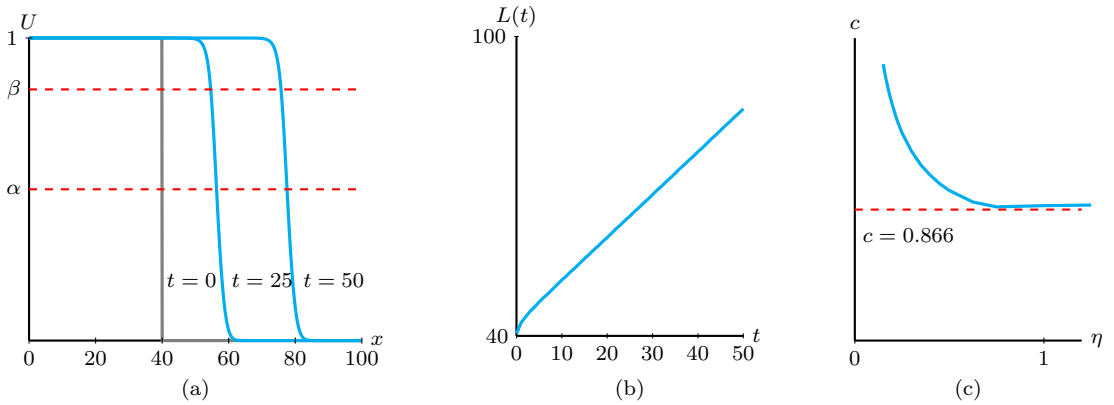

Fig. 2 (a) shows the evolution of a Heaviside initial condition to a smooth travelling wave solution obtained by simulating (2) with (3) and (5) with parameters $D_i = 0.25$, $D_g = 0.05$ and $\lambda = 0.75$. We use a finite difference method with space step $\delta x = 0.1$, time step $\delta t = 0.01$ and no-flux boundary conditions. Notice that $D(U) = 0$ at $\alpha = 0.5$ and $\beta \approx 0.83$. (b) measures the position of the wave $L(t)$ by looking for the left-most leading edge point where U is smaller than 10^{-5}, indicating that the solution is travelling at a constant speed $c = 0.864$. (c) gives the wave speed as a function of the initial condition $U(x, 0) = 1/2 + \tanh(-\eta(x - 40))/2$. Notice that as η grows to infinity this initial condition limits to the Heaviside initial condition used for the simulation in (a), and the wave speed converges to $c \approx 0.864$. The minimum wave speed $c^* = 2\sqrt{\lambda D_i} \approx 0.866$ (9).

the *comparison method* introduced by [4]. Related studies proved the existence of travelling wave solutions for a similar range of speeds for nonlinear diffusion-reaction equations with different $D(U)$ and different $R(U)$: [31] studied (2) with a logistic kinetic term and a nonlinear diffusivity function satisfying

$$D(0) = 0 \quad \text{and} \quad D(0) > 0 \quad \text{for all} \quad U \in (0, 1].$$

[29] studied (2) with a logistic kinetic term and a nonlinear diffusivity function satisfying

$$D(U) > 0 \quad \text{in} \quad (0, \theta) \quad \text{and} \quad D(U) < 0 \quad \text{in} \quad U \in (\theta, 1), \tag{8}$$

for some given $\theta \in (0, 1)$ and with $D(0) = D(\theta) = D(1) = 0$. In addition, [30] studied (2) with (8) and a bistable kinetic term satisfying

$$R(0) = R(\phi) = R(1) = 0, \quad R(U) < 0 \quad \text{in} \quad U \in (0, \phi) \quad \text{and} \quad R(U) > 0 \quad \text{in} \quad U \in (\phi, 1).$$

In this manuscript, we show the following result:

Theorem 1 *Model (2) with (3) and (5) and $D_i > 4D_g$ supports smooth monotone nonnegative travelling wave solutions for*

$$c \geq 2\sqrt{\lambda D_i} =: c^*. \tag{9}$$

This theorem agrees with the result of [13], and because of the specific nonlinear diffusivity function, we can further extend their results. Moreover, instead of the comparison method used by [13], we use a geometric approach to prove the existence of travelling wave solutions. This geometric approach has the advantage that it can also be used to study shock-fronted travelling wave solutions [16, 17, 46]. While shock-fronted travelling wave solutions are not the focus in this manuscript, we show in the final section that they do exist for (5) with different $D(U)$, see Figure 10a in Section 4.3. The lower bound c^* in Theorem 1 is often called the minimum wave speed as it represents the monotone nonnegative travelling wave solutions with the lowest wave speed [32]. Numerical simulations show that (2) with (3) and (5) indeed support smooth travelling wave solutions even though the nonlinear diffusivity function goes negative. Moreover, the speed relates to the initial condition, and the wave speed converges to the minimum wave speed c^* as the initial

condition limits to the Heaviside initial condition, see Figure 2. We will also show the connection between the existence of smooth monotone nonnegative travelling wave solutions, the spectrum of the travelling wave solutions, and the minimum wave speed c^*.

This manucript is organised as follows. We prove Theorem 1 in Section 2 by using desingularisation techniques [3] and detailed phase plane analysis which have not been applied to (2) before. In Section 3, we determine the spectral properties of the travelling wave solutions and show how the minimum wave speed c^* is related to absolute instabilities [22, 37, 40]. Some interesting results for different nonlinear diffusivity functions with the same kinetic term (5) are discussed in Section 4. Here, we also discuss the implications of the analytical results for the discrete model.

2 Existence of travelling wave solutions

2.1 Transformation and Desingularisation

A travelling wave solution of (2) is a solution of the form $u(x-ct,t)$ that travels with constant speed c and constant wave shape, and that asymptotes to 1 as $x \to -\infty$ and to 0 as $x \to \infty$. We only consider positive wave speeds since (2) with (3) and (5) is monostable with a Fisher-KPP imprint, that is, $U \equiv 1$ is a PDE stable solution of (2), while $U \equiv 0$ is a PDE unstable solution. We introduce the travelling wave coordinate $z = x - ct$, where $z \in \mathbb{R}$, and write (2) in its travelling wave coordinate

$$\frac{\partial U}{\partial t} = \frac{\partial}{\partial z}\left(D(U)\frac{\partial U}{\partial z}\right) + c\frac{\partial U}{\partial z} + R(U). \tag{10}$$

A travelling wave solution to (2) is now a stationary solution to (10), that is, $\partial U/\partial t = 0$, and (10) simplifies to a second-order ordinary differential equation (ODE)

$$\frac{d}{dz}\left(D(u)\frac{du}{dz}\right) + c\frac{du}{dz} + R(u) = 0, \tag{11}$$

with asymptotic boundary conditions $\lim_{z\to-\infty} u = 1$ and $\lim_{z\to\infty} u = 0$. We use a dynamical systems approach to analyse (11). Upon introducing $p := D(u)du/dz$, it can be written as a system of first-order ODEs

$$\begin{cases} D(u)\dfrac{du}{dz} = p, \\ D(u)\dfrac{dp}{dz} = -cp - D(u)R(u). \end{cases} \tag{12}$$

Note that $p > 0$ if $du/dz < 0$ and $D(u) < 0$. Thus, while we expect that the derivative of a travelling wave solution is always negatvie, p is not necessarily always negative. Travelling wave solutions of (2) now correspond to heteroclinic orbits of (12) connecting $(1,0)$ to $(0,0)$. However, (12) is singular as $D(u)$ is zero for $u = \alpha$ and $u = \beta$, see (7). That is, we have two *walls of singularities* $u = \alpha$ and $u = \beta$ [16, 33, 46]. On these walls of singularities the right hand sides of (2) also dissappear if $p = 0$. That is, each wall of singularities has one (potential) *hole in the wall* [16, 33, 46]. In system (12), the holes are at $(\alpha, 0)$ and $(\beta, 0)$. To remove the singularities, we desingularise system (12) by introducing a stretched variable ξ satisfying $D(u)d\xi = dz$ [3, 32, 36]. Subsequently, system (12) becomes

$$\begin{cases} \dfrac{du}{d\xi} = p, \\ \dfrac{dp}{d\xi} = -cp - D(u)R(u). \end{cases} \tag{13}$$

When $D(u) > 0$, $d\xi/dz > 0$ and therefore trajectories on the phase planes of (12) and (13) have the same moving directions. In contrast, when $D(u) < 0$, $d\xi/dz < 0$ and trajectories on the two phase planes are in the opposite direction, see Figure 3. Therefore, heteroclinic orbits of (12) connecting

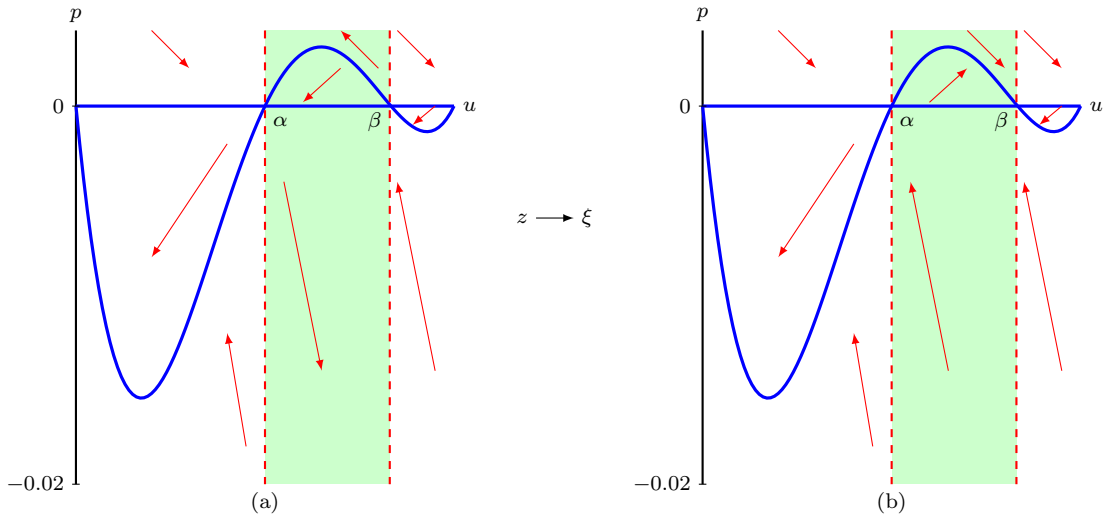

Fig. 3 (a) is the phase plane of system (12) with parameters $D_i = 0.25$, $D_g = 0.05$, $\lambda = 0.75$ and $c = 0.866$. The vertical dashed lines are the walls of singularities $u = \alpha$ and $u = \beta$ and the solid blue lines are nullclines. Red arrows show the moving direction of trajectories. (b) is the phase plane of system (13) for the same parameter values and red lines are nullclines. For u in between α and β, the moving direction of the trajectories is opposite compared to (a), while the moving direction is the same for $u < \alpha$ and $u > \beta$.

$(1,0)$ to $(0,0)$ crossing the holes in the walls $(\alpha,0)$ and $(\beta,0)$, if they exist, are transformed and separated to heteroclinic orbits connecting $(1,0)$ to $(\beta,0)$, $(\alpha,0)$ to $(\beta,0)$ and $(\alpha,0)$ to $(0,0)$ of (13) and *vice versa*. Next, we will prove the existence of these heteroclinic orbits in system (13) for a range of wave speeds c.

2.2 Phase plane analysis of the desingularised system

We first study the desingularised system (13). It has nullclines $p = 0$ and

$$p = -\frac{D(u)R(u)}{c}. \tag{14}$$

The intersections of the two nullclines give four equilibrium points: $(0,0), (1,0), (\alpha,0), (\beta,0)$.

Lemma 1 *The equilibrium points* $(1,0)$ *and* $(\alpha,0)$ *are saddles. The equilibrium point* $(0,0)$ *is a stable node if*

$$c \geq 2\sqrt{D(0)R'(0)} = 2\sqrt{\lambda D_i} = c^*, \tag{15}$$

and a stable spiral otherwise. The equilibrium point $(\beta,0)$ *is a stable node if*

$$c \geq 2\sqrt{D'(\beta)R(\beta)}, \tag{16}$$

and a stable spiral otherwise.

Proof The Jacobian of system (13) is

$$J(u,p) = \begin{pmatrix} 0 & 1 \\ -F(u) & -c \end{pmatrix}, \quad \text{where} \quad F(u) := (D(u)R(u))'. \tag{17}$$

The Jacobian has eigenvalues and eigenvectors

$$\lambda_{\pm} = \frac{-c \pm \sqrt{c^2 - 4F(u)}}{2}, \quad E_{\pm} = (1, \lambda\pm).$$

For the equilibrium point $(1, 0)$ this reduces to

$$\lambda_{1\pm} = \frac{-c \pm \sqrt{c^2 - 4D(1)R'(1)}}{2}, \quad E_{1\pm} = (1, \lambda_{1\pm}). \tag{18}$$

The eigenvalues $\lambda_{1\pm}$ are real and negative since $D(1) = D_g > 0$ and $R'(1) = -\lambda < 0$. Thus $(1, 0)$ is a saddle.

Similarly, the Jacobian of the equilibrium point $(\alpha, 0)$ has eigenvalues and eigenvectors

$$\lambda_{\alpha\pm} = \frac{-c \pm \sqrt{c^2 - 4D'(\alpha)R(\alpha)}}{2}, \quad E_{\alpha\pm} = (1, \lambda_{\alpha\pm}). \tag{19}$$

Knowing that $D'(\alpha) < 0$ and $R(\alpha) > 0$, $\lambda_{\alpha+}$ is real and positive and $\lambda_{\alpha-}$ is real and negative. Thus $(\alpha, 0)$ is a saddle.

The Jacobian of the equilibrium point $(0, 0)$ has eigenvalues and eigenvectors

$$\lambda_{0\pm} = \frac{-c \pm \sqrt{c^2 - 4D(0)R'(0)}}{2}, \quad E_{0\pm} = (1, \lambda_{0\pm}). \tag{20}$$

The eigenvalues $\lambda_{0\pm}$ are real and negative if (15) holds since $D(0) = D_i > 0$ and $R'(0) = \lambda > 0$. Thus equilibrium point $(0, 0)$ is a stable node if (15) holds. Otherwise, $\lambda_{0\pm}$ are complex-valued with negative real parts and $(1, 0)$ is a stable spiral.

Similarly, the Jacobian of equilibrium point $(\beta, 0)$ has eigenvalues and eigenvectors

$$\lambda_{\beta\pm} = \frac{-c \pm \sqrt{c^2 - 4D'(\beta)R(\beta)}}{2}, \quad E_{\beta\pm} = (1, \lambda_{\beta\pm}). \tag{21}$$

The eigenvalues $\lambda_{\beta\pm}$ are real and negative if (16) holds since $D'(\beta) > 0$ and $R(\beta) > 0$. Thus the equilibrium point $(\beta, 0)$ is a stable node if (16) holds. Otherwise, $\lambda_{\beta\pm}$ are complex-valued with negative real parts and $(\beta, 0)$ is a stable spiral. □

Lemma 2 *For $D_i > 4D_g$, the thresholds of conditions (15) and (16) give*

$$c^* > 2\sqrt{D'(\beta)R(\beta)}. \tag{22}$$

Proof The right hand side of (22) is given by

$$2\sqrt{D'(\beta)R(\beta)} = 2\sqrt{3\lambda(D_i - D_g)\beta(1-\beta)(\beta-\alpha)}.$$

Since $c^* = 2\sqrt{\lambda D_i}$, proving relation (22) is equivalent to proving

$$D_i > 3(D_i - D_g)\beta(1-\beta)(\beta-\alpha),$$

which is equivalent to proving

$$\frac{D_i}{D_i - D_g} > 3\beta(1-\beta)(\beta-\alpha). \tag{23}$$

Knowing that $2/3 < \beta < 1$ and $0 < \beta - \alpha < 2/3$ gives $3\beta(1-\beta)(\beta-\alpha) < 2/3$. Since $D_i > 4D_g$, we have that $D_i/(D_i - D_g) > 1$ since $D_i > D_i - D_g$. Hence, (23) holds and thus (22) holds. □

For $c < c^*$, $(0,0)$ becomes a spiral node and hence we expect trajectories approaching $(0,0)$ to become negative which in the end would lead to travelling wave solutions become negative. Therefore, we now assume that $c \geq c^*$. To prove the existence of heteroclinic orbits between the equilibrium points, we construct invariant regions in the phase plane from which trajectories cannot leave, so that the Poincaré-Bendixson theorem can be applied [21], see Figure 4. The slope of nullcline (14) is $\chi(u) = -1/(cF(u))$, where $F(u)$ is given by (17), while the slope of the unstable eigenvector of $(1,0)$ is λ_{1+}, see (18). We thus have

$$\begin{aligned}\lambda_{1+} - \chi(1) =& \frac{-c + \sqrt{c^2 - 4D(1)R'(1)}}{2} + \frac{1}{c}D(1)R'(1) \\ =& \frac{c\sqrt{c^2 - 4D(1)R'(1)} - \left(c^2 - 2D(1)R'(1)\right)}{2c} \\ =& \frac{\sqrt{c^4 - 4c^2D(1)R'(1)} - \sqrt{c^4 - 4c^2D(1)R'(1) + 4\left(D(1)R'(1)\right)^2}}{2} < 0.\end{aligned} \tag{24}$$

That is, the unstable eigenvector of $(1,0)$ has a smaller slope than nullcline (14) at $(1,0)$. In other words, the trajectory leaving $(1,0)$ with decreasing u initially lies above the nullcline (14).

Similarly, the slope of the unstable eigenvector of $(\alpha,0)$ is $\lambda_{\alpha+}$, see (19). We have, after similar computation as (24), $\lambda_{\alpha+} - \chi(\alpha) < 0$. Thus, the unstable eigenvector of $(\alpha,0)$ has a smaller slope than nullcline (14) at $(\alpha,0)$. Therefore, the trajectory leaving $(\alpha,0)$ with decreasing u initially lies above the nullcline (14), while the trajectory leaving $(\alpha,0)$ with increasing u initially lies below the nullcline (14).

Under condition (15), the least negative slope of the stable eigenvectors of equilibrium point $(0,0)$ is λ_{0+}, see (20). This gives, after a similar computation as (24), $\lambda_{0+} - \chi(0) < 0$. Thus, both eigenvectors of $(0,0)$ have slopes that are more negative than nullcline (14) at $(0,0)$. In other words, the eigenvectors of $(0,0)$ initially lie under the nullcline (14) for $u > 0$.

Similarly, under condition (16), the least negative slope of the stable eigenvectors of $(\beta,0)$ is $\lambda_{\beta+}$, see (21). This gives $\lambda_{\beta+} - \chi(\beta) < 0$. Thus, both eigenvectors have slopes that are more negative than nullcline (14) at $(\beta,0)$. Therefore, the trajectory moving in $(\beta,0)$ with decreasing u initially lies under the nullcline (14) for $u > \beta$, while they lie above the nullcline (14) for $u < \beta$, see also Figure 4.

Next, we consider the region $\mathcal{R}_1$ bounded by $p = 0$, $u = \alpha$ and a straight line l_1 through $(0,0)$ with a negative slope μ_1. We aim to prove that for $c \geq c^*$, there always exists a slope μ_1 so that no trajectories in region $\mathcal{R}_1$ can cross through its boundaries. Trajectories starting on $p = 0$ have negative vertical directions since $du/d\xi = p = 0$ and $dp/d\xi = -D(u)R(u) < 0$ for $u \in (0,\alpha)$. Thus, trajectories in $\mathcal{R}_1$ cannot cross through $p = 0$. Trajectories starting on $u = \alpha$ with negative p values point into region $\mathcal{R}_1$ since $du/d\xi = p < 0$ and $dp/d\xi = -cp > 0$. Trajectories starting on l_1 satisfy $p = \mu_1 u$, and they point into $\mathcal{R}_1$ only if

$$\left.\frac{dp}{du}\right|_{p=\mu_1 u} = -c - \frac{D(u)R(u)}{\mu_1 u} \leq \mu_1, \quad \text{for} \quad u \in (0,\alpha).$$

After rearranging and recalling that $\mu_1 < 0$, we obtain

$$\mu_1(\mu_1 + c) \leq -\frac{D(u)R(u)}{u} = -\lambda D(u)(1-u), \quad \text{for} \quad u \in (0,\alpha). \tag{25}$$

Lemma 3 *For $c \geq c^*$, there exists a μ_1 such that inequality (25) is valid for any $u \in (0,\alpha)$.*

Proof Proving inequality (25) is equivalent to proving

$$\mu_1(\mu_1 + c) \leq -\lambda \sup_{u\in(0,\alpha)} D(u)(1-u). \tag{26}$$

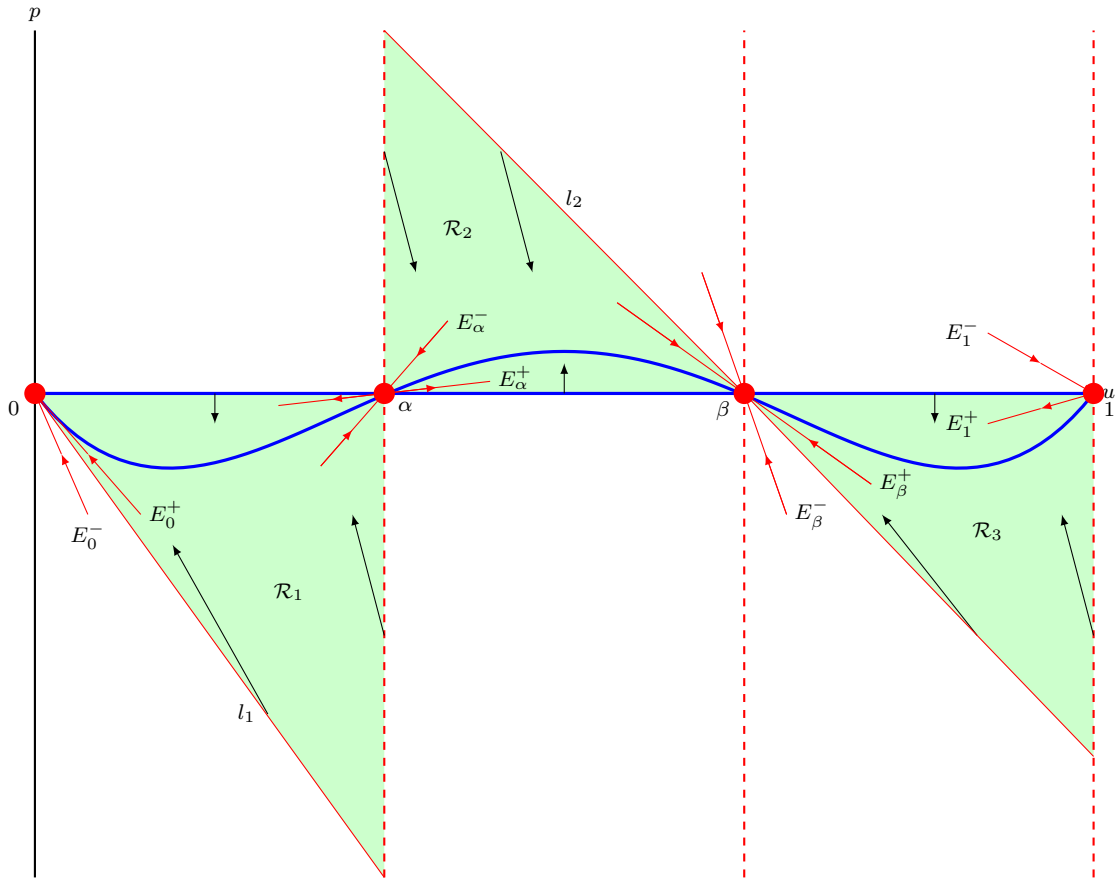

Fig. 4 A qualitative phase plane of system (13). The three dashed lines are $u = \alpha$, $u = \beta$ and $u = 1$. The blue lines are the nullclines $p = 0$ and $p = -D(u)R(u)/c$. Region $\mathcal{R}_1$ is bounded by $p = 0$, $u = \alpha$ and a straight line l_1 with negative slope passing through $(0, 0)$. Region $\mathcal{R}_2$ is bounded by $p = 0$, $u = \alpha$ and a straight line l_2 with negative slope passing through $(\beta, 0)$. Region $\mathcal{R}_3$ is bounded by $p = 0$, $u = 1$ and l_2.

The left hand side of inequality (26) is minimal when $\mu_1 = -c/2$. Setting $\mu_1 = -c/2$ and substituting into inequality (26) gives a lower bound for the speed

$$c_1 = 2\sqrt{\lambda} \sup_{u\in(0,\alpha]} \sqrt{D(u)(1-u)}, \tag{27}$$

such that (26) holds for $c \geq c_1$. The right hand side of (27) gives

$$2\sqrt{\lambda} \sup_{u\in(0,\alpha)} \sqrt{D(u)(1-u)} = 2\sqrt{\lambda D(0)} = 2\sqrt{\lambda D_i},$$

since $D(u)$ and $(1-u)$ are both decreasing functions on $u \in (0, \alpha)$. Thus, $c_1 = c^*$. Hence, for $c \geq c^*$, inequality (26) is valid for $\mu_1 = -c/2$. □

Knowing that for $c \geq c^*$ inequality (25) is valid, trajectories on l_1 with $\mu_1 = -c/2$ point into region $\mathcal{R}_1$. Thus, based on the Poincaré-Bendixson theorem [21], the trajectory leaving from the equilibrium point $(\alpha, 0)$ with decreasing u and decreasing p must connect with the equilibrium point $(0, 0)$ without going negative in u.

Similarly, we consider the region $\mathcal{R}_2$ bounded by $p = 0$, $u = \alpha$ and a straight line l_2 through $(\beta, 0)$ with a negative slope μ_2, and the region $\mathcal{R}_3$ bounded by $p = 0$, $u = 1$ and l_2. Trajectories starting on $p = 0$ have positive vertical directions for $u \in (\alpha, \beta)$ since $du/d\xi = p = 0$ and $dp/d\xi = -D(u)R(u) > 0$ and they have negative vertical directions since for $u \in (\beta, 1)$, $du/d\xi = 0$ and $dp/d\xi = -D(u)R(u) < 0$. Trajectories starting on $u = \alpha$ with positive p point into region $\mathcal{R}_2$ since $du/d\xi = p > 0$ and $dp/d\xi = -cp < 0$. Similarly, trajectories starting on $u = 1$ with negative p point into region $\mathcal{R}_3$. In addition, requiring the existence of a slope μ_2 such that trajectories starting on l_2 point into regions $\mathcal{R}_2$ and $\mathcal{R}_3$ leads to the condition

$$\mu_2(\mu_2 + c) \leq -\frac{D(u)R(u)}{u - \beta} = -3(D_i - D_g)(u - \alpha)R(u), \quad \text{for} \quad u \in (\alpha, 1). \tag{28}$$

Lemma 4 *For $c \geq c^*$, there exists a μ_2 such that inequality (25) is valid for any $u \in (\alpha, 1)$.*

Proof The proof of Lemma 4 is analogous to the proof of Lemma 3 and we will omit some of the details. Again, there exist a lower bound c_2

$$c_2 = 2\sqrt{3(D_i - D_g)} \sup_{u \in (\alpha, 1)} \sqrt{(u - \alpha)R(u)},$$

such that (28) holds for $c \geq c_2$. Next, we show that $c_2 < c^*$. That is, we show that

$$2\sqrt{\lambda D_i} > 2\sqrt{3(D_i - D_g)} \sup_{u \in (\alpha, 1)} \sqrt{(u - \alpha)R(u)}.$$

This is equivalent to proving $D_i/(D_i - D_g) > 3u(1 - u)(u - \alpha)$ for $u \in (\alpha, 1)$. Noticing that $u - \alpha < 2/3$, and $u(1 - u) \leq 1/4$, we obtain $3u(1 - u)(u - \alpha) < 1/2$. Subsequently, we have

$$\frac{D_i}{D_i - D_g} > 1 > \frac{1}{2} > 3u(1 - u)(u - \alpha),$$

since $D_i > 4D_g$ by assumption. Thus, $c_2 < c^*$. □

Knowing that for $c \geq c^*$ the inequality (28) is valid, trajectories on l_2 in between α and β point into region $\mathcal{R}_2$. Thus, based on the Poincaré-Bendixson theorem [21], the trajectory leaving from the equilibrium point $(\alpha, 0)$ with increasing u and increasing p must connect with the equilibrium point $(\beta, 0)$. Analogously, the trajectory leaving from the equilibrium point $(1, 0)$ with decreasing u and decreasing p must connect with the equilibrium point $(\beta, 0)$.

In summary, for $c \geq c^*$ there exist heteroclinic orbits connecting $(1, 0)$ to $(\beta, 0)$, $(\alpha, 0)$ to $(\beta, 0)$ and $(\alpha, 0)$ to $(0, 0)$ in system (13). Since trajectories in $u \in (0, \alpha) \cup (\beta, 0)$ in system (12) have the same moving direction as in system (13), there exist trajectories connecting $(1, 0)$ to the hole in the wall $(\beta, 0)$ and trajectories connecting the hole in the wall $(\alpha, 0)$ to $(0, 0)$ in system (12). For $u \in (\alpha, \beta)$, trajectories of system (12) have the opposite moving direction compared to (12). The trajectory leaving from $(\alpha, 0)$ with increasing u, positive p and connecting to $(\beta, 0)$ in system (13) becomes a trajectory leaving from $(\beta, 0)$ with decreasing u, positive p and connecting to $(\alpha, 0)$ in system (12). Thus, there exists an orbit connecting $(\beta, 0)$ to $(\alpha, 0)$ in system (12). Combining the above, we get that for $c \geq c^*$, there exists a heteroclinic orbit with $u \geq 0$ connecting $(1, 0)$ to $(0, 0)$ passing through holes in the walls $(\alpha, 0)$ and $(\beta, 0)$ in system (12). Hence, there exist smooth monotone travelling wave solutions of (2) with positive speed $c \geq c^*$. This completes the proof of Theorem 1.

For $2\sqrt{D'(\beta)R(\beta)} < c < c^*$ the equilibrium point $(\beta, 0)$ is still a stable node, while $(0, 0)$ is a stable spiral, see Lemma 1. We can use similar techniques as above to show that system (13) still possesses heteroclinic orbits connecting $(1, 0)$ to $(\beta, 0)$, $(\alpha, 0)$ to $(\beta, 0)$ and $(\alpha, 0)$ to $(0, 0)$, see also Figure 5. However, this latter heteroclinic orbit now spirals into $(0, 0)$. Consequently, also for $2\sqrt{D'(\beta)R(\beta)} < c < c^*$ there exists a heteroclinic orbit connecting $(1, 0)$ to $(0, 0)$ passing through

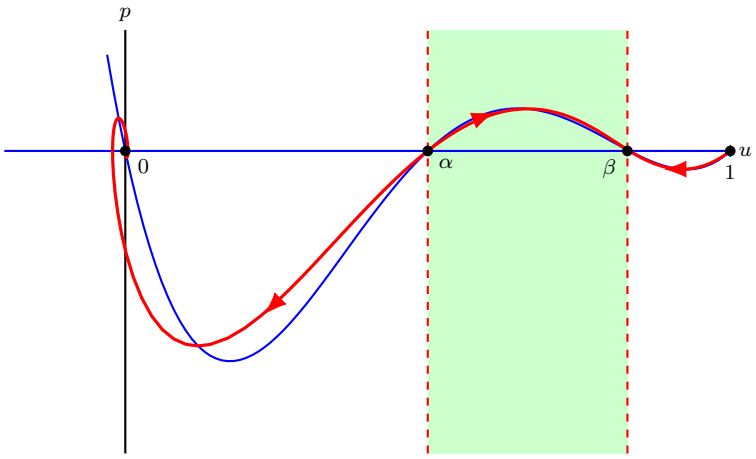

Fig. 5 Phase plane of system (13) with parameters $D_i = 0.25$, $D_g = 0.05$, $\lambda = 0.75$ and $c = 0.4$. The latter is smaller than $c^* \approx 0.866$ but larger than $2\sqrt{D'(\beta)R(\beta)} \approx 0.289$. The blue lines are the nullclines $p = 0$ and $p = -D(u)R(u)/c$. The red lines are the heteroclinic orbits connecting $(0,0)$, $(\alpha,0)$, $(\beta,0)$, and $(1,0)$.

holes in the walls $(\alpha, 0)$ and $(\beta, 0)$ in system (12). However, these correspond to smooth travelling wave solutions of (2) with (3) and (5) that are not monotone and instead oscillate around 0. These solutions are not feasible as U represents the population density in the discrete model and thus cannot be negative.

3 Stability analysis

We showed that, similar to the Fisher-KPP equation [18, e.g.], (2) with (3) and (5) supports smooth travelling wave solutions for $c > 2\sqrt{D'(\beta)R(\beta)}$, but that only the travelling wave solutions with $c \geq c^*$ (9) are feasible. The minimal wave speed for the Fisher-KPP equation is closely related to the onset of absolute instabilities. Roughly speaking, absolute instabilities imply that perturbations to a travelling wave solution will grow for all time and at every point in space [40]. These instabilities are related to the absolute spectrum of the travelling wave solution and are fully determined by the asymptotic behaviour ($z \to \pm\infty$) of the travelling wave solution [22, 37]. The travelling wave solutions of (2) with (3) and (5) as constructed in Section 2 asymptote to 0 and 1 and the nonlinear diffusivity function $D(U)$ is positive near $U = 0$ and $U = 1$, see (6). That is, near these points (2) with (3) and (5) has a Fisher-KPP imprint and we therefore expect that the minimal wave speed c^* of (2) is also closely related to the onset of absolute instabilities. In other words, we expect that the travelling wave solutions of (2) with (3) and (5) are absolutely unstable for $2\sqrt{D'(\beta)R(\beta)} < c < c^*$. Therefore, we expect perturbations to these travelling wave solutions to always grow and we will never observe them in, for instance, numerical simulations. Consequently, while (2) with (3) and (5) support these unfeasible travelling wave solutions that go negative, they will never be observed and thus do not effect the feasibility of the model.

Below, we briefly describe how to determine the absolute spectrum of a travelling wave solution, for a more detailed and complete mathematical description, we refer to [8, 22, 37]. To determine the absolute spectrum of a travelling wave solution $\hat{u}(z)$, we add a small perturbation $q(z,t)$ to the travelling wave solution and determine how this perturbation evolves under the PDE in its moving frame. That is, we substitute $u(z,t) = \hat{u}(z) + q(z,t)$ into (10) and, upon ignoring higher-order

perturbative terms $\mathcal{O}(q^2)$, we get

$$\frac{\partial q}{\partial t} = \mathcal{L}q\,, \qquad \mathcal{L} := D(\hat{u})\frac{\partial^2}{\partial z^2} + \left(2D'(\hat{u})\frac{d\hat{u}}{dz} + c\right)\frac{\partial}{\partial z} + \left(D'(\hat{u})\frac{d^2\hat{u}}{dz^2} + D''(\hat{u})\left(\frac{d\hat{u}}{dz}\right)^2 + R'(\hat{u})\right).$$

The associated eigenvalue problem, which is obtained by setting $q(z,t) = e^{\Lambda t}q(z)$, is given by

$$\mathcal{L}q = \Lambda q. \tag{29}$$

The spectral stability of the travelling wave solution $\hat{u}$ is now determined by the spectrum of the linear operator $\mathcal{L}$, that is, the $\Lambda \in \mathbb{C}$ for which $\mathcal{L} - \Lambda$ is not invertible. In particular, if the spectrum is in the open left half plane, or the origin, then we call the travelling wave solution $\hat{u}$ spectrally stable and unstable otherwise. This spectrum naturally breaks up into two sets, the point spectrum and the essential spectrum [22, 37]. Roughly speaking, the essential spectrum of the travelling wave solution deals with instabilities at infinity and it is related to the spectrum of the background linear operator $\mathcal{L}$ as $z \to \pm\infty$, while the point spectrum deals with the stability of the actual wave front.

Obviously, the spectral properties of $\mathcal{L}$ depend on the space we allow the perturbations q to be taken from. A natural choice is the space of square integrable functions whose first (weak) derivative (in z) is also square integrable, that is, the Sobolev space $\mathbb{H}^1(\mathbb{R})$. Another choice is the related weighted space $\mathbb{H}^1_\nu(\mathbb{R})$ defined as $q \in \mathbb{H}^1_\nu(\mathbb{R})$ if and only if $e^{\nu z}q \in \mathbb{H}^1(\mathbb{R})$ [22, 38]. For positive ν the weight forces q to decay at a rate faster than $e^{-\nu z}$ as $z \to \infty$, while it is allowed to grow exponentially, but at a rate less than $e^{-\nu z}$, as $z \to -\infty$. That is, the weight provides information whether the travelling wave solution is more sensitive to perturbations at plus or minus infinity [8]. The weighting of $\mathbb{H}^1(\mathbb{R})$ does not influence the point spectrum of $\mathcal{L}$, however, it does shift the essential spectrum [22]. That is, a travelling wave solution can be unstable with respect to perturbations in $\mathbb{H}^1(\mathbb{R})$, while it is stable with respect to perturbations in an appropriately weighted space $\mathbb{H}^1_\nu(\mathbb{R})$. This is, for instance, the case for the Fisher-KPP equation and a particular Keller-Segel model [8, 9]. The absolute spectrum of a travelling wave solution, which is strictly speaking not always part of the spectrum, is not affected by the weighting of the space and gives an indication on how far the essential spectrum can be weighted (as the absolute spectrum is always to the left of the rightmost boundary of the essential spectrum [8]). In other words, if the absolute spectrum of a travelling wave solution contains part of the right half plane then the essential spectrum cannot be weighted into the open left half plane and the travelling wave solution is said to be absolutely unstable.

The eigenvalue problem (29) can be written as a system of first order ODEs

$$\mathcal{T}(\Lambda)\begin{pmatrix} q \\ s \end{pmatrix} := \left(\frac{d}{dz} - A(z;\Lambda)\right)\begin{pmatrix} q \\ s \end{pmatrix} = 0\,, \quad \text{where} \quad A(z;\Lambda) := \begin{pmatrix} 0 & 1 \\ \mathcal{B} & \mathcal{C} \end{pmatrix},$$

with

$$\mathcal{B} = -\frac{1}{D(\hat{u})}\left(D'(\hat{u})\frac{d^2\hat{u}}{dz^2} + D''(\hat{u})\left(\frac{d\hat{u}}{dz}\right)^2 + R'(\hat{u}) - \Lambda\right), \quad \mathcal{C} = -\frac{1}{D(\hat{u})}\left(2D'(\hat{u})\frac{d\hat{u}}{dz} + c\right).$$

The unweighted essential spectrum and the absolute spectrum of the operator $\mathcal{L}$ are determined by the asymptotic behaviour of the operator $\mathcal{T}(\Lambda)$ since the operator is a relatively compact perturbation of the operator when you plug in $z = \pm\infty$ [22]. Therefore, we define the asymptotic matrices

$$A_+(\Lambda) := \lim_{z\to+\infty} A(z,\Lambda) = \begin{pmatrix} 0 & 1 \\ \dfrac{-R'(0)+\Lambda}{D(0)} & -\dfrac{c}{D(0)} \end{pmatrix},$$

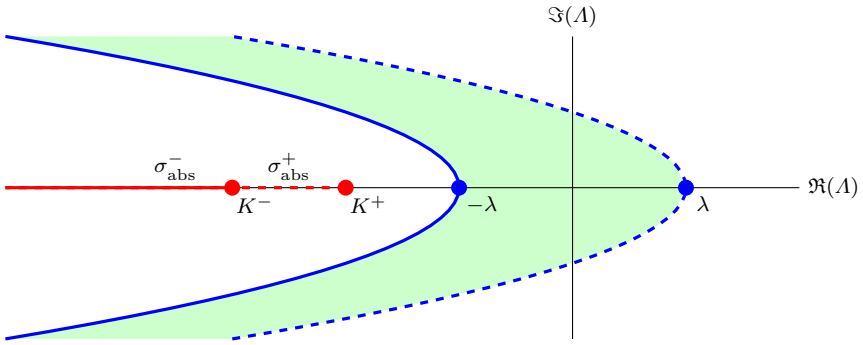

Fig. 6 The unweighted essential spectrum and the absolute spectrum of the linear operator $\mathcal{L}$ for $c > c^*$. The boundary of the unweighted essential spectrum is determined by the dispersion relations of A_+ (dashed blue curve) and A_- (solid blue curve) and the green region is the interior of the unweighted essential spectrum. The solid red line is the absolute spectrum σ^-_{abs} (33), while the dashed red line is the absolute spectrum σ^+_{abs} (32).

and

$$A_-(\Lambda) := \lim_{z\to-\infty} A(z,\Lambda) = \begin{pmatrix} 0 & 1 \\ \dfrac{-R'(1)+\Lambda}{D(1)} & -\dfrac{c}{D(1)} \end{pmatrix}.$$

More specifically, for the problem at hand the boundary of the unweighted essential spectrum of $\mathcal{L}$ is determined by those Λ for which $A_\pm(\Lambda)$ has a purely imaginary eigenvalue.

In contrast, the absolute spectrum at $\pm\infty$ is determined by those Λ for which the eigenvalues of $A_\pm(\Lambda)$ have the same real part [37]. The eigenvalues of A_+ are

$$\mu_+^\pm = \frac{-c \pm \sqrt{c^2 - 4D(0)R'(0) + 4D(0)\Lambda}}{2D(0)}, \tag{30}$$

and those of A_- are

$$\mu_-^\pm = \frac{-c \pm \sqrt{c^2 - 4D(1)R'(1) + 4D(1)\Lambda}}{2D(1)}. \tag{31}$$

Hence, the boundary of the unweighted essential spectrum is given by the so-called dispersion relations

$$\Lambda_+ = -D(0)k^2 + ick + R'(0), \quad \text{and} \quad \Lambda_- = -D(1)k^2 + ick + R'(1),$$

where $k \in \mathbb{R}$ and where $\mu_\pm^\pm = ik$ are the purely imaginary spatial eigenvalue of $A_\pm$. These dispersion relations form two parabolas, opening leftward and intersecting the real axis at $R'(0) = \lambda > 0$ and $R'(1) = -\lambda < 0$, see Figure 6. That is, all travelling wave solutions of (2) with (3) and (5) have unweighted essential spectrum in the right half plane.

From (30) we get that the absolute spectrum at $+\infty$ is given by

$$\sigma^+_{\text{abs}} = \left\{ \Lambda \in \mathbb{R} \;\middle|\; \Lambda < -\frac{c^2}{4D(0)} + R'(0) = -\frac{c^2}{4D_i} + \lambda =: K^+ \right\}. \tag{32}$$

Similarly, from (31) we get that the absolute spectrum at $-\infty$ is given by

$$\sigma^-_{\text{abs}} = \left\{ \lambda \in \mathbb{R} \;\middle|\; \Lambda < -\frac{c^2}{4D(1)} + R'(1) = -\frac{c^2}{4D_g} - \lambda =: K^- \right\}. \tag{33}$$

That is, σ^-_{abs} is always fully contained in the open left half plane including the origin, while σ^+_{abs} is only fully contained in the open left half plane including the origin for $c \geq c^* = 2\sqrt{\lambda D_i}$, see Figure 6.

In conclusion, a travelling wave solution with speed $2\sqrt{D'(\beta)R(\beta)} < c < c^*$ is absolutely unstable and no weights exist to shift its unweighted essential spectrum into the open left half plane. In contrast, the absolute spectrum of a travelling wave solution with speed $c \geq c^*$ is fully contained in the open left half plane including the origin and weights can be found that shift the unweighted essential spectrum into this region.

Remark 1 To fully establish spectral stability of the operator $\mathcal{L}$, we also need to determine the point spectrum of $\mathcal{L}$ and show that it is contained in the open left half plane including the origin when $c \geq c_*$ provided our perturbations stay in an appropriately chosen Hilbert space $\mathcal{X}$. With this in mind, we define

$$w(z) := D(\hat{u})q(z)e^{\int c/(2D(\hat{u}(t)))dt}. \tag{34}$$

Then if $\mathcal{L}q = \Lambda q$ (29) we have that w will solve

$$\mathcal{M}w(z) := D(\hat{u})w_{zz} + \left(R'(\hat{u}) - \frac{c\left(c + 2D'(\hat{u})\hat{u}_z\right)}{4D(\hat{u})}\right)w(z) = \Lambda w(z).$$

We have thus reduced the problem to showing that $\mathcal{M}$ is negative semi-definite on some appropriately chosen Hilbert space $\mathcal{X}$. Unfortunately, the natural choice for such a Hilbert space in these problems is the one with"inner product"

$$(u, v) := \int \frac{uv}{D(\hat{u})}dz,$$

but the sign change in $D(\hat{u})$ means that this is actually no longer an inner product (it is strictly negative for a localised pulse near where $D(\hat{u})$ is negative for instance).

However, if we instead work with the desingularised system (13), then for a perturbation $\tilde{q}$ about $\hat{u}$, linearising gives the eigenvalue problem for the linearised desingularised system

$$\tilde{q}_{\xi\xi} + c\tilde{q}_\xi + F(\hat{u})\tilde{q} = \Lambda\tilde{q}\,, \tag{35}$$

where $F(u)$ is defined in (17). The standard Liouville transformation $\tilde{w}(\xi) := \tilde{q}(\xi)e^{c\xi/2}$ now does lead to a self adjoint eigenvalue problem in terms of $\tilde{w}(\xi)$

$$\tilde{w}_{\xi\xi} + \left(F(\hat{u}) - \frac{c^2}{4}\right)\tilde{w}(\xi) = \Lambda\tilde{w}(\xi)\,.$$

Here, one can show explicitly that the operator

$$\tilde{\mathcal{M}} := \frac{d^2}{d\xi^2} + \left(F(\hat{u}) - \frac{c^2}{4}\right)$$

is negative semi-definite precisely when $c \geq c_*$. Indeed, as we are assuming that $D_i > 4D_g$, the potential term in $\tilde{\mathcal{M}}$ satisfies

$$\left(F(\hat{u}) - \frac{c^2}{4}\right) < \frac{1}{4}\left(-c^2 + \lambda D_i(4 - 32\hat{u} + 63\hat{u}^2 - 36\hat{u}^3)\right)$$

and the polynomial term $4 - 32\hat{u} + 63\hat{u}^2 - 36\hat{u}^3$ has a maximum value of 4 when $\hat{u} \in [0, 1]$ (at $\hat{u} = 0$). So, we have that $F(\hat{u}) - c^2/4 \leq 0$ when $c \geq c_* = 2\sqrt{\lambda D_i}$. Thus, $\tilde{\mathcal{M}}$ is a negative semidefinite operator in the space of perturbations which decay faster than $e^{c\xi}$, that is, $\mathbb{H}^1_c$. This is usually referred to as a transient instability in the stability literature [37, 40].

Lastly, we remark that given what was just shown, the only remaining step in the proof of stability of these travelling wave solutions for $c \geq c_*$ is how to relate the eigenvalue problem of the desingularised system (35) to the spectrum of the operator $\mathcal{L}$. Due to the singular nature of the

operator, it is unclear how to even define the 'natural' Hilbert spaces which should act as domains for the original linearised problem. Further, the weighting given in (34) involves a nonlinear, singular exponential weight, and to the best of our knowledge there is no such work which describes the dynamic effects of stability or instability in these cases. So, we cannot even say whether we would have only a transient instability even if we could show that the 'natural' operator was negative definite on an appropriate domain.

4 Summary and future work

4.1 Summary of results

We started this manuscript with a lattice-based discrete model reflecting the differences in individual and collective cell behaviour introduced in [20]. Based on [20], the discrete model has the continuous description (2) obtained by using truncated Taylor series in the continuum limit. Our analysis focused on the case where $D_i > 4D_g$ so that we can obtain a convex nonlinear diffusivity function $D(U)$, given by (3) which changes sign twice in our domain of interest. Furthermore, the assumption of equal proliferation rates and zero death rates leads to a logistic kinetic term $R(U)$, given by (5). The associated numerical simulations of (2) with (3) and (5), see Figure 2, provided evidence of the existence of smooth monotone travelling wave solutions. To study these travelling wave solutions of (2), we used a travelling wave coordinate $z = x - ct$ and looked for stationary solutions in the moving frame. Consequently, (2) was transformed into the singular second-order ODE (11) which we transformed into a singular system of first-order ODEs (12). To remove the singularities, we used the stretched variable $D(u)d\xi = dz$ and transformed (12) into system (13). Next, we analysed the phase plane of the desingularised system (13) and proved the existence of heteroclinic orbits connecting the equilibrium points $(0,0), (\alpha,0), (\beta,0)$ and $(1,0)$ for wave speeds $c \geq c^*$, given by (9). Subsequently, based on the relation between the phase planes of (12) and (13), we proved the existence of a heteroclinic orbit in (12) connecting the equilibrium points $(1,0)$ and $(0,0)$ passing through $(\alpha,0)$ and $(\beta,0)$, that are special points on the phase plane called a hole in the wall of singularities. That is, we proved the existence of smooth monotone travelling wave solutions of (2) for $c \geq c^*$. In the end, we showed that the travelling wave solutions of (2) with wave speeds $c < c^*$ are absolutely unstable, which in turn explained that the numerical simulations only provided travelling wave solutions with wave speeds $c \geq c^*$.

Based on our analysis, one-dimensional agent density profiles will eventually spread with a speed $c \geq c^*$ if the two types of agents have equal proliferation rates, zero death rates and different diffusivities satisfying $D_i > 4D_g$. Notice that $c^* = 2\sqrt{\lambda D_i}$, hence, the lowest speed for the travelling wave only relates to the diffusivity of individuals and is independent of the diffusivity of the gouped agents. That is, the diffusivity of grouped agents which is smaller than that of isolated agents ($D_i > 4D_g$) does not give restrictions for the lowest speed of the moving front. Consequently, we infer that the speed of invasion processes for organisms, for instance, cells, is mainly determined by the behaviour of individuals. Furthermore, the Fisher-KPP equation also has a minimum wave speed for the existence of smooth monotone travelling wave solutions [14, 25]. Hence, a discrete mechanism of invasion processes considering the differences in individual and collective behaviours can lead to the similar macroscopic behaviour as the discrete mechanism with no differences in isolated and grouped agents.

4.2 Smooth travelling wave solutions for positive $D(U)$

If $D_i < 4D_g$, then the nonlinear diffusivity function $D(U)$ is positive for $U \in [0,1]$, see Figure 7a. Thus the corresponding system of first-order ODEs (12) is not singular, and the nullcline $p = -D(u)R(u)/c$ does not cross u-axis, see Figure 7b. In other words, $(0,0)$ and $(1,0)$ are the

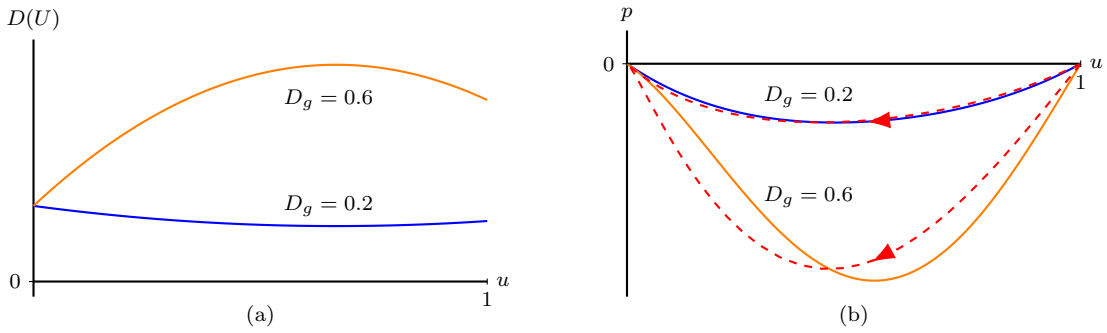

Fig. 7 (a) shows $D(U)$ with $D_i = 0.25$ and two different D_g. (b) gives the corresponding phase planes of system (12) for $\lambda = 0.75$, $c = 1$, $D_i = 0.25$, $D_g = 0.2$ and $D_g = 0.6$, respectively. The two solid curves are the nullclines $p = -D(u)R(u)/c$ with $D_g = 0.2$ (blue curve) and $D_g = 0.6$ (orange curve), respectively. The red dashed lines are the corresponding heteroclinic orbits representing travelling wave solutions in (2).

only equilibrium points. Following the same method as applied in Section 2.2, we obtain the lower bound

$$S_1 = \sup_{u\in(0,1)} 2\sqrt{\frac{D(u)R(u)}{u}} = \sup_{u\in(0,1)} 2\sqrt{\lambda(1-u)D(u)},$$

such that there exist smooth monotone travelling wave solutions of (2) for $c \geq S_1$. The origin is still a stable node for $c \geq 2\sqrt{\lambda D_i} := S_2$ and $S_1 \geq S_2$. So, if $S_1 \neq S_2$, $c \geq S_1$ is only a sufficient condition because there may exist smooth monotone travelling wave solutions of (2) for wave speeds $S_2 \leq c < S_1$. Thus, we can only conclude that the minimum wave speed is in the range

$$S_2 \leq \hat{c} \leq S_1, \tag{36}$$

such that there exist smooth monotone nonnegative travelling wave solutions of (2) for $c \geq \hat{c}$. Note that the minimum wave speed $\hat{c}$ can be different from the minimum wave speed c^* in Theorem 1, and Lemma 2 does not necessarily hold.

This estimate is consistent with the result in [31] obtained based on the *comparison method* introduced by [4]. The corresponding numerical simulations also give the expected results, see Figure 8. [47] obtained an asymptotic travelling wave solution for a PDE motivated by polymer diffusion with a positive nonlinear diffusivity function and logistic kinetics for wave speeds greater than a minimum wave speed which is greater than S_2. This is consistent with the estimate of the minimum wave speed in (36). For solutions with an asymptotic wave speed equal to S_2, the front of the travelling wave is called a *pulled front*; for solutions with asymptotic speeds greater than S_2, the front of the travelling wave is called a *pushed front* [35]. Unravelling the differences in wave speed selection remains to be explored.

4.3 Shock-fronted travelling waves

In Section 2, we mainly considered the equilibrium point $(0, 0)$ as a stable node in the phase plane of system (13). With $(0, 0)$ a stable node, $(\beta, 0)$ is also a stable node based on (22). However, (22) does not hold for any convex $D(U)$ which changes sign twice. For instance, for

$$\hat{D}(U) = (U - 0.1)(U - 0.3), \tag{37}$$

condition (15) and condition (16) become

$$c \geq 2\sqrt{\hat{D}(0)R'(0)} = 0.3, \quad c \geq 2\sqrt{\hat{D}'(0.3)R(0.3)} \approx 0.355.$$

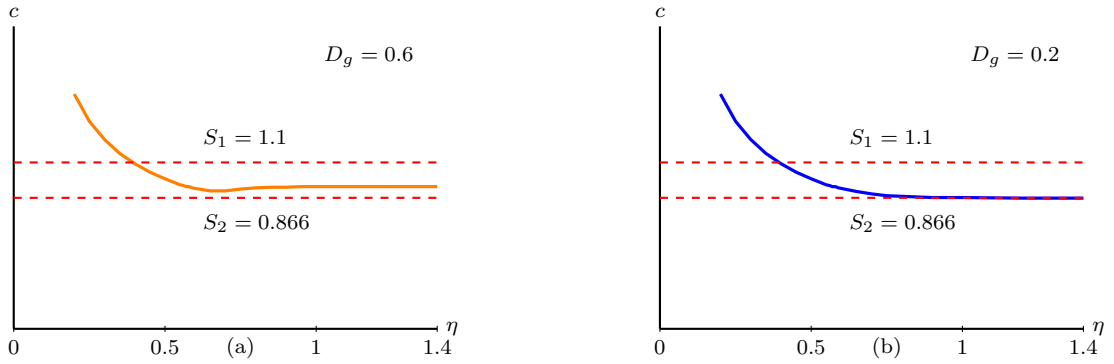

Fig. 8 (a) gives the wave speed as a function of the initial condition $U(x,0) = 1/2 + \tanh(-\eta(x-40))/2$. Notice that as η grows to infinity this initial condition limits to the Heaviside initial condition. Parameters are $\lambda = 0.75$, $D_i = 0.25$ and $D_g = 0.6$. The wave speed reaches its minimum which is between S_1 and S_2 and then converges to a bigger value which is still between S_1 and S_2. In (b), $D_g = 0.2$ while the other parameters are the same. In this case, the wave speed converges to S_2.

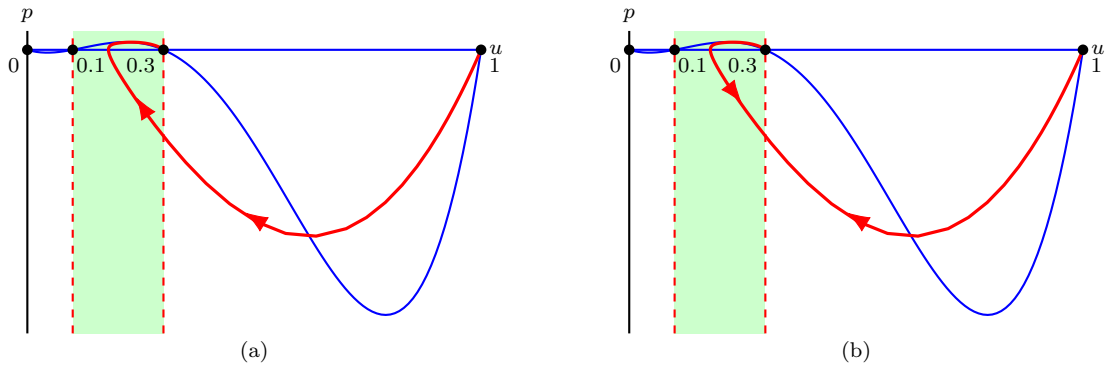

Fig. 9 (a) is the phase plane of the desingularised system (13) with $\hat{D}(u)$, $c = 0.3$ and $\lambda = 0.75$. The vertical dashed lines are the wall of singularities at $u = 0.1$ and $u = 0.3$. The blue lines are the nullclines $p = 0$ and $p = -D(u)R(u)/c$. The red line is the heteroclinic orbit connecting $(1,0)$ to $(0.3,0)$. (b) is the phase plane of system (12) with $\hat{D}(u)$, $c = 0.3$ and $\lambda = 0.75$. The vertical dashed lines are the walls of singularities $u = 0.1$ and $u = 0.3$. The blue lines are the nullclines $p = 0$ and $p = -D(u)R(u)/c$. The red line shows the opposite moving directions of the same trajectory in (a) on different sides of the wall of singularities $u = 0.3$.

With the nonlinear diffusivity function $\hat{D}(U)$, the equilibrium point $(0,0)$ is a stable node and the equilibrium point $(\beta,0)$ is a stable spiral for speeds $0.3 < c < 0.355...$ in (13). In this case, only shock-fronted travelling wave solutions of (2) can exist since (13) no longer possesses heteroclinic orbits connecting to $(\beta,0)$ that do not cross the walls of singularities, see Figure 9. The corresponding numerical simulation of (2) indeed gives a shock-fronted travelling wave solution with a speed $c = 0.3$, see Figure 10.

It is not a surprise to see shock-fronted travelling wave solutions in negative nonlinear diffusion equations. Shocks in negative nonlinear diffusion equations with no kinetic terms have been studied in the context of many physical phenomena, such as the movement of moisture in partially saturated porous media [11]; the motion of nanofluids [26] and these kinds of PDEs also arise in the study of Cahn-Hilliard models [48]. Numerical simulations of (2) with nonlinear diffusivity function (3) and Allee kinetics (4) also lead to shock-fronted solutions, see [20]. In addition, Allee kinetics support shock-fronted travelling wave solutions for reaction-diffusion-advection equations with small diffusion coefficients [39, 45]. The analysis of shock-fronted travelling wave solutions in

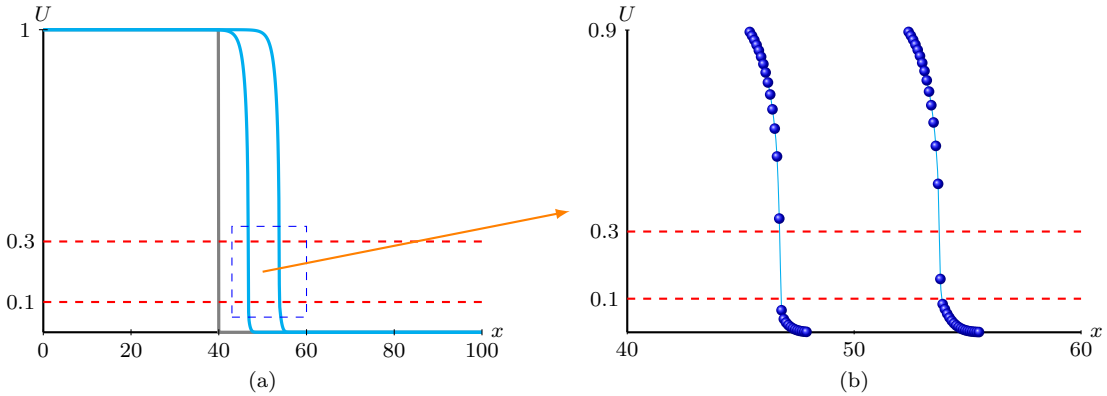

Fig. 10 (a) shows the evolution of a Heaviside initial condition to a smooth travelling wave solution obtained by simulating (2) with (37) and (5) with $\lambda = 0.75$ at $t = 0$, $t = 25$ and $t = 50$. Notice that $D(U) = 0$ at $\alpha = 0.1$ and $\beta = 0.3$. The travelling wave solution eventually has a constant positive speed, $c = 0.3$. (b) amplifies the region around the shock. Blue dots represent the numerical simulations of the corresponding travelling wave solutions which indicate the existence of a shock.

nonlinear diffusion-reaction equations with generic diffusivity functions and logistic kinetics is left for future work.

Acknowledgements The authors would like to thank P Davis and M Wechselberger for fruitful discussions.

References

[1] Allee W, Bowen ES (1932) Studies in animal aggregations: Mass protection against colloidal silver among goldfishes. Journal of Experimental Zoology 61(2):185–207

[2] Anguige K, Schmeiser C (2009) A one-dimensional model of cell diffusion and aggregation, incorporating volume filling and cell-to-cell adhesion. Journal of Mathematical Biology 58(3):395

[3] Aronson DG (1980) Density-dependent interaction-diffusion systems. In: Dynamics and Modelling of Reactive Systems, Elsevier, pp 161–176

[4] Aronson DG, Weinberger HF (1978) Multidimensional nonlinear diffusion arising in population genetics. Advances in Mathematics 30(1):33–76

[5] Bramson M, Calderoni P, De Masi A, Ferrari P, Lebowitz J, Schonmann RH (1986) Microscopic selection principle for a diffusion-reaction equation. Journal of Statistical Physics 45(5-6):905–920

[6] Codling EA, Plank MJ, Benhamou S (2008) Random walk models in biology. Journal of the Royal Society Interface 5(25):813–834

[7] Courchamp F, Clutton-Brock T, Grenfell B (1999) Inverse density dependence and the Allee effect. Trends in Ecology & Evolution 14(10):405–410

[8] Davis PN, van Heijster P, Marangell R (2017) Absolute instabilities of travelling wave solutions in a Keller–Segel model. Nonlinearity 30(11):4029

[9] Davis PN, van Heijster P, Marangell R (2018) Spectral stability of travelling wave solutions in a Keller–Segel model. Applied Numerical Mathematics (in press), DOI https://doi.org/10.1016/j.apnum.2018.05.008

[10] Deroulers C, Aubert M, Badoual M, Grammaticos B (2009) Modeling tumor cell migration: From microscopic to macroscopic models. Physical Review E 79(3):031917

[11] DiCarlo DA, Juanes R, LaForce T, Witelski TP (2008) Nonmonotonic traveling wave solutions of infiltration into porous media. Water Resources Research 44(2):W02406

[12] Druckenbrod NR, Epstein ML (2007) Behavior of enteric neural crest-derived cells varies with respect to the migratory wavefront. Developmental Dynamics 236(1):84–92

[13] Ferracuti L, Marcelli C, Papalini F (2009) Travelling waves in some reaction-diffusion-aggregation models. Advances in Dynamical Systems and Applications 4(1):19–33

[14] Fife PC (2013) Mathematical Aspects of Reacting and Diffusing Systems, vol 28. Springer Science & Business Media

[15] Fisher RA (1937) The wave of advance of advantageous genes. Annals of Eugenics 7(4):355–369

[16] Harley K, van Heijster P, Marangell R, Pettet GJ, Wechselberger M (2014) Existence of traveling wave solutions for a model of tumor invasion. SIAM Journal on Applied Dynamical Systems 13(1):366–396

[17] Harley K, van Heijster P, Marangell R, Pettet GJ, Wechselberger M (2014) Novel solutions for a model of wound healing angiogenesis. Nonlinearity 27(12):2975

[18] Harley K, van Heijster P, Marangell R, Pettet GJ, Wechselberger M (2015) Numerical computation of an Evans function for travelling waves. Mathematical Biosciences 266:36–51

[19] Johnston ST, Simpson MJ, Baker RE (2012) Mean-field descriptions of collective migration with strong adhesion. Physical Review E 85(5):051922

[20] Johnston ST, Baker RE, McElwain DLS, Simpson MJ (2017) Co-operation, competition and crowding: a discrete framework linking Allee kinetics, nonlinear diffusion, shocks and sharp-fronted travelling waves. Scientific Reports 7:42134

[21] Jordan DW, Smith P (1999) Nonlinear Ordinary Differential Equations: An Introduction to Dynamical Systems, vol 2. Oxford University Press, USA

[22] Kapitula T, Promislow K (2013) Spectral and dynamical stability of nonlinear waves. Springer

[23] Khain E, Sander LM, Schneider-Mizell CM (2007) The role of cell-cell adhesion in wound healing. Journal of Statistical Physics 128(1-2):209–218

[24] Khain E, Katakowski M, Hopkins S, Szalad A, Zheng X, Jiang F, Chopp M (2011) Collective behavior of brain tumor cells: The role of hypoxia. Physical Review E 83(3):031920
[25] Kolmogorov A, Petrovsky I, Piscounov N (1937) Étude de l'équation de la diffusion avec croissance de la quantité de matière et son application à un problème biologique. Moscow University Mathematics Bulletin 1:1–25
[26] Landman KA, White LR (2011) Terraced spreading of nanofilms under a nonmonotonic disjoining pressure. Physics of Fluids 23(1):012004
[27] Larson DA (1978) Transient bounds and time-asymptotic behavior of solutions to nonlinear equations of Fisher type. SIAM Journal on Applied Mathematics 34(1):93–104
[28] Mack RN, Simberloff D, Mark Lonsdale W, Evans H, Clout M, Bazzaz FA (2000) Biotic invasions: Causes, epidemiology, global consequences, and control. Ecological Applications 10(3):689–710
[29] Maini PK, Malaguti L, Marcelli C, Matucci S (2006) Diffusion-aggregation processes with mono-stable reaction terms. Discrete and Continuous Dynamical Systems Series B 6(5):1175–1189
[30] Maini PK, Malaguti L, Marcelli C, Matucci S (2007) Aggregative movement and front propagation for bi-stable population models. Mathematical Models and Methods in Applied Sciences 17(9):1351–1368
[31] Malaguti L, Marcelli C (2003) Sharp profiles in degenerate and doubly degenerate Fisher-Kpp equations. Journal of Differential Equations 195(2):471–496
[32] Murray JD (2002) Mathematical Biology: I. An Introduction. Mathematical Biology, Springer
[33] Pettet GJ, McElwain DLS, Norbury J (2000) Lotka-Volterra equations with chemotaxis: Walls, barriers and travelling waves. Mathematical Medicine and Biology: A Journal of the IMA 17(4):395–413
[34] Poujade M, Grasland-Mongrain E, Hertzog A, Jouanneau J, Chavrier P, Ladoux B, Buguin A, Silberzan P (2007) Collective migration of an epithelial monolayer in response to a model wound. Proceedings of the National Academy of Sciences 104(41):15988–15993
[35] van Saarloos W (2003) Front propagation into unstable states. Physics Reports 386(2-6):29–222
[36] Sánchez-Garduño F, Maini PK (1994) Existence and uniqueness of a sharp travelling wave in degenerate non-linear diffusion Fisher-Kpp equations. Journal of Mathematical Biology 33(2):163–192
[37] Sandstede B (2002) Stability of travelling waves. In: Handbook of Dynamical Systems, vol 2, Elsevier, pp 983–1055
[38] Sattinger D (1977) Weighted norms for the stability of traveling waves. Journal of Differential Equations 25(1):130–144
[39] Sewalt L, Harley K, van Heijster P, Balasuriya S (2016) Influences of allee effects in the spreading of malignant tumours. Journal of Theoretical Biology 394:77–92
[40] Sherratt JA, Dagbovie AS, Hilker FM (2014) A mathematical biologistâ$^{\mathrm{TM}}$s guide to absolute and convective instability. Bulletin of Mathematical Biology 76(1):1–26
[41] Simpson MJ, Landman KA, Hughes BD (2010) Cell invasion with proliferation mechanisms motivated by time-lapse data. Physica A: Statistical Mechanics and its Applications 389(18):3779–3790
[42] Simpson MJ, Landman KA, Hughes BD, Fernando AE (2010) A model for mesoscale patterns in motile populations. Physica A: Statistical Mechanics and its Applications 389(7):1412–1424
[43] Simpson MJ, Towne C, McElwain DLS, Upton Z (2010) Migration of breast cancer cells: Understanding the roles of volume exclusion and cell-to-cell adhesion. Physical Review E 82(4):041901
[44] Simpson MJ, Haridas P, McElwain DLS (2014) Do pioneer cells exist? PLOS ONE 9(1):e85488
[45] Wang Y, Shi J, Wang J (2018) Persistence and extinction of population in reaction–diffusion–advection model with strong Allee effect growth. Journal of Mathematical Biology (online

only) DOI https://doi.org/10.1007/s00285-019-01334-7
[46] Wechselberger M, Pettet GJ (2010) Folds, canards and shocks in advection–reaction–diffusion models. Nonlinearity 23(8):1949
[47] Witelski TP (1994) An asymptotic solution for traveling waves of a nonlinear-diffusion Fisher's equation. Journal of Mathematical Biology 33(1):1–16
[48] Witelski TP (1995) Shocks in nonlinear diffusion. Applied Mathematics Letters 8(5):27–32